Evaluation of photocatalytic and corrosion properties of green synthesized zinc oxide nanoparticles

S. Ramamoorthy[1,3,*] , S. Surendhiran[2], D. Senthil Kumar[3], G. Murugesan[3],
M. Kalaiselvi[1], S. Kavisree[1], S. Muthulingam[4], and S. Murugesan[5]

[1] *Department of Physics, Vivekanandha Arts and Science College for Women, Salem, Tamil Nadu 637 303, India*

[2] *Centre for Nanoscience and Technology, K.S. Rangasamy College of Technology, Namakkal, Tamil Nadu 637 215, India*

[3] *Department of Physics, Vel Tech Rangarajan Dr.Sagunthala R&D Institute of Science and Technology, Avadi, Chennai, Tamil Nadu 600 062, India*

[4] *Department of Chemistry, Sri Ramakrishna College of Arts and Science (SRCAS), Coimbatore, Tamil Nadu 641 006, India*

[5] *Department of Physics, Vivekanandha College of Arts and Sciences for Women (Autonomous), Namakkal, Tamil Nadu 637 205, India*

ABSTRACT

Zinc oxide (ZnO) nanoparticles were prepared from Neem plant extracts using the green synthesis method. The single-phase formation of the compound without any impurities was observed from the X-ray diffraction studies. The presence of spherical-shaped ZnO nanoparticles within the size range of 23–40 nm was observed from SEM micrographs and EDX, revealing 63.34% zinc and 36.66% oxygen. DLS studies showed the average particle size of the prepared sample to be around 27.81 nm at the d_{50} range. The prepared material had an optical bandgap of around 3.24 eV. The photodegradation studies proved the better photocatalytic behavior of the prepared sample. Corrosion studies revealed that the prepared ZnO nanoparticles were less corrosive in comparison with zinc plates.

1 Introduction

Several novel syntheses have been adopted in the last few years to prepare nanoparticles with appreciable size, morphology, and desired physical properties [1]. The miniature size of nanoparticles ranging from 1 to 100 nm has made it a potential candidate for several applications in the field of medicinal chemistry, atomic physics and other technologies [2]. Based on dimensions, nanoparticles are classified into zero, one and 2-dimensional nanostructures [3]. Among them, quantum dots with zero dimensions play a major role in biological fields as nanomedicines and nanocarriers [4]. Zinc, gold, and silver nanoparticles have been considered as suitable materials for wide applications due to their superior photocatalytic property, long-term performance, and non-toxicity [5]. Food and drug administration of the US (FDA) has reported that ZnO nanoparticles are less toxic in comparison with other metal oxides [6].

Address correspondence to E-mail: ramjothymani@gmail.com

ZnO nanoparticles possess a wide bandgap (3.37 eV), binding energy (60 meV), and exceptional antibacterial properties which makes them suitable for several technological applications [7, 8]. Due to its intriguing properties, ZnO nanoparticles are used for several applications in the field of photocatalysts, biosensors, optoelectronic devices, and water purification [9]. Earlier reports have shown that in comparison with chemical route techniques ZnO nanoparticles prepared by the green synthesized method showed better antibacterial effects at lower concentrations [10, 11]. The superior antibacterial properties of ZnO nanoparticles make it a potential candidate for several applications in the various fields of drug delivery, antibacterial treatments, anticancer treatments, agriculture [12–16]. Among the several approaches for the synthesis of nanoparticles, biosynthesis methods have been adopted due to their low cost and environmentally friendly design [17]. Greener synthesis of nanoparticles is found to be more advantageous in comparison with chemical methods due to its environmentally friendly nature, better stabilization, and control over crystal growth [18, 19].

Compared with other chemical methods of synthesis, greener synthesis of nanoparticles has better stabilization and control over crystal growth. Recently zinc oxide nanoparticles have been synthesized from many plant extracts, of these *Azadirachta indica* (Neem) is a traditional medicinal plant of wide application in Ayurveda, Siddha, Unani, and homeopathy [20]. Due to the presence of highly active components in this plant, both gel and leaf of *A. indica* have been used for pharmacological applications [21]. Jeeva Lakshmi et al. in 2012 reported the synthesis and antimicrobial effect of zinc oxide nanoparticles from hot and cold plant extracts and observed a significant change in the particle size and properties [22].

Metals are mainly used in petrochemicals, oil and gas, steel, and other industries, in all these industries interaction of metals with the environment, may damage its property and lead to corrosion [23]. The consequences due to corrosion can be minimized by the usage of corrosive inhibitors, metallic coatings, and cathodic protection [24]. Mainly organic and polymer-coated materials are used as corrosion inhibitors, but these are expensive and make adverse effects on our environment [25]. So the development of eco-friendly cost-effective corrosion inhibitors from green sources plays an important role in these

industries. Recently many studies have proved that nanomaterials from different plant extracts, fruits, and seeds can act as an efficient corrosion inhibitor in the different mediums [25]. This is because plant extract acts as a capping and stabilizing agent is also adsorbed on the surface of the metal, and this will block the metal surface and thereby prevent corrosion [26]. In biogenic synthesis, plant extract can reduce the usage of harmful chemicals and also minimize the cost of production [27].

In the present work, ZnO nanoparticles were synthesized by the green route technique and their structural, optical, photocatalytic, and corrosion behavior were analyzed.

2 Materials & methods

Fresh neem plant leaves were collected and washed in distilled water, the aqueous extract is prepared by boiling 25 g of fresh leaves in 100 mL sterilized water at 65 °C for 20 min. The aqueous extract is filtered after being stirred in a magnetic stirrer until the coloration shifts from orange to brown. The plant extract is stored in a cold environment to avoid decomposition. ZnO nanoparticles are prepared by combining 25 mL of a stored extract with 25 mL of zinc acetate. The prepared solution is stirred well using a stirrer and the pH 7.0 is maintained by adding 0.5 M sodium hydroxide (NaOH) at room temperature to get a white precipitate. The collected sample is washed several times with water and ethanol to remove impurities using a centrifuge. Finally, the precipitate is dried in an oven at 60 °C and calcined at 400 °C for 1 h in a muffle furnace.

3 Characterization techniques

The crystalline structure of the prepared ZnO nanoparticles was elucidated by an X-ray diffractometer (XRD; X'Pert PRO, PANalytical operated at 40 kV and 30 mA with Cu Kαsource). The XRD pattern had been studied within the angle range from 20 to 80°.

The average particle size distribution of the prepared material is determined by using the dynamic light scattering (DLS) technique (Nanophox Sympatec, Germany) by illuminating light of a wavelength of 633 nm. The surface morphology of the prepared

material is viewed by a field-emission scanning electron microscope (FESEM; JSM-6790 LS; JEOL) and the compositional analysis has been carried out using an EDX analyzer.

The optical behavior of the prepared ZnO nanoparticles was analyzed by using a UV–Visible (UV–Vis) spectrophotometer (Agilent Cary 8454, Singapore) at wavelengths from 180 to 800 nm of the electromagnetic spectral region. The bandgap energy of the prepared ZnO nanoparticles is calculated using the Tauc relation from the absorption spectra [28–31].

3.1 Sample preparation for photocatalytic activity

The photocatalytic dye degradation activity of the prepared sample was dispensed by assessing the degradation of methyl orange (MO) and Rhodamine-B (RB) dye under a constant UV light irradiation. The photocatalytic dye degradation for the prepared samples was measured by the following formula [31],

$$\eta = \frac{C_0 - C_t}{C_0} \times 100$$

Here, η is the degradation calculation, C_0 is the early absorbance of dye (at 00 min); C_t is the variation in absorbance of the dye at after time intervals of the degradation.

3.2 Sample preparation for corrosion studies

The anticorrosive behavior of the prepared ZnO nanoparticles was analyzed by corrosion studies. About 15 mg of prepared ZnO nanoparticles were mixed with Polyvinylidene difluoride (PVDF) and N-methyl-2-pyrrolidone (NMP) at 80:15:5 weight proportions to create suspension. The slurry was additionally coated on the Zn metal plate surface by adopting the doctor's blade technique [32]. The coated plate was dried within the hot-air oven at 353 K for 1 h and used for corrosion studies beneath 3.5% NaCl electrolyte.

4 Results & discussion

4.1 XRD analysis

The powder XRD pattern of the prepared ZnO nanoparticles is shown in Fig. 1a. The characteristic

peaks confirmed the formation of a hexagonal wurtzite crystal structure with three most preferred orientations (1 0 0), (0 0 2), and (1 0 1), all of which are very close to the standard JCPDS Card No: 36-1451 [14]. The XRD pattern of the prepared ZnO nanoparticles shows that no characteristic impurity peaks have been obtained. This clearly shows that the prepared nanoparticles are free from contamination. The Debye–Scherrer equation was used to calculate the size of the crystallites. The calculated crystallite size of the prepared ZnO nanoparticle is 11.3 nm. Rietveld refinement of the powder XRD peaks were carried out by using FULLPROF software [33, 34]. The refinement plot of the prepared ZnO nanoparticles is shown in Fig. 1b and it can be observed that the Bragg peaks match well with the XRD data.
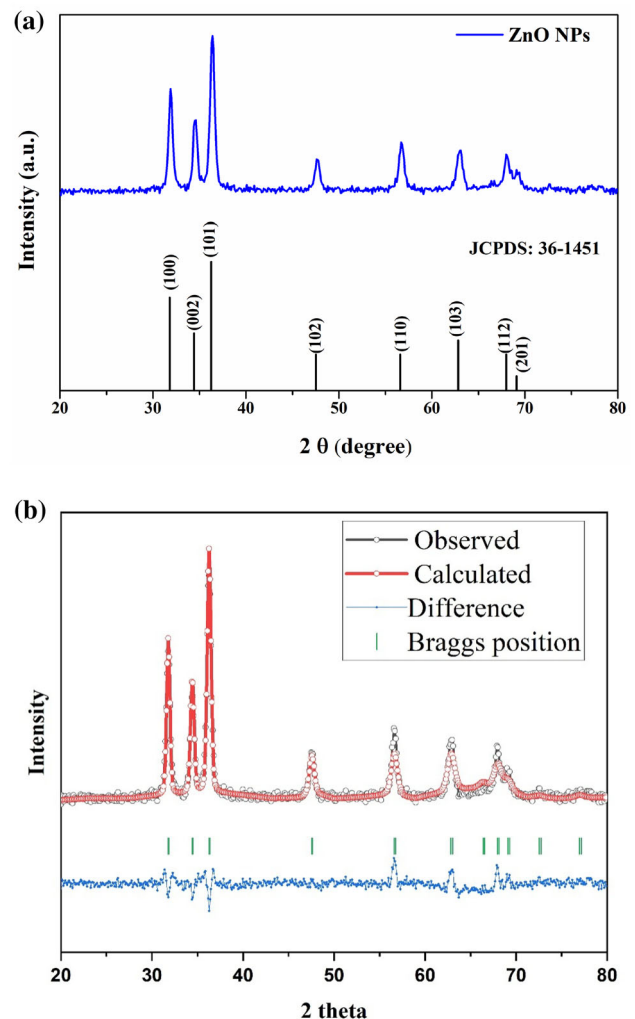

Fig. 1 a Powder X-ray diffraction pattern of the ZnO nanoparticles. b Refinement plot of the ZnO nanoparticles

4.2 UV–Vis analysis

The UV–Vis absorption spectra of ZnO nanoparticles are shown in Fig. 2. The UV absorption peak was found to be around 375 nm and the bandgap of the prepared nanoparticles was calculated from the Tauc plot. The calculated energy bandgap from the Tauc plot (Fig. 3a, b) is within the range from 3.1 to 3.3 eV, which is consistent with previous results [9, 20] The calculated energy bandgap from the Tauc plot for direct transition is 3.24 eV and the indirect transition is 3.14 eV.

4.3 Morphological studies

The morphology and elemental compositional analysis of the green synthesized zinc oxide nanoparticles were ascertained by FESEM and EDX, respectively (Fig. 4a, b). SEM micrographs (Fig. 4a) revealed the presence of spherical-shaped ZnO nanoparticles with very small-sized clusters in the range between 23 and 40 nm. EDX (Fig. 4b) revealed the presence of 63.34% Zinc and 36.66% of oxygen, no traces of impurities were observed.

4.4 DLS studies

The particle size of the prepared nanoparticles was exploited by dynamic light-weight scattering. The particle size distribution of the ZnO nanoparticles is shown in Fig. 5, it signifies that the particle size ranges from 16.19 (d_{10}) to 45.84 (d_{90}) nm. The average particle is found to be 27.81 nm.
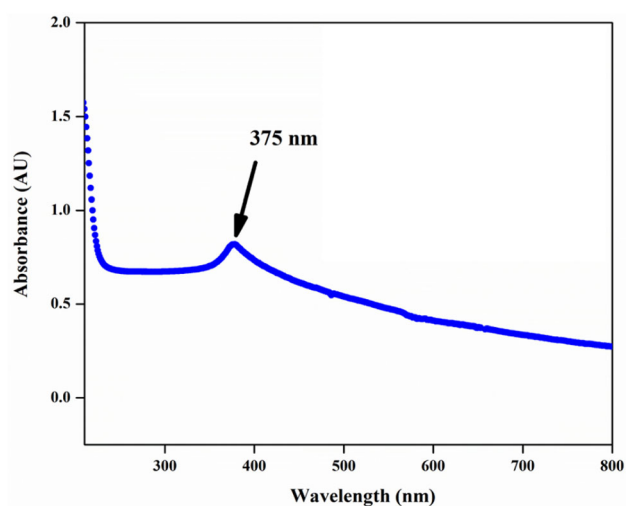

Fig. 2 UV–Vis spectrum for the prepared ZnO nanoparticles

4.5 Photocatalytic activity

Photocatalytic activity is recorded by using prepared nanoparticles as photocatalyst in Rhodamine-B (RB) and methyl orange (MO) aqueous solution. The absorption spectra (Fig. 6a, c) of MO and RB dye were recorded by illuminating UV radiation at regular intervals (30, 60, 90, and 120 min).

Irradiation of UV light on ZnO leads to the transfer of electrons from the valence band (VB) to the conduction band (CB) leaving behind positive holes in VB. The electrons transferred are termed as photogenerated electrons, the holes in VB and the photogenerated electrons in CB are accountable for the photodegradation [35, 36]. Generally, three steps are involved in a photocatalytic process (i) electron–hole pairs generation (ii) electron–hole pair separation, and (iii) generation of high active hydroxyl radicals due to the surface redox reactions [37].

The absorption spectra during the photodegradation of MO for different times (0, 30, 60, 90, 120 min) is shown in Fig. 6a. A sharp decrease in the absorption peak is observed at around 538 nm and tends to diminish after 120 min of irradiation of UV light.

The temporal variation in the UV–Vis spectra during the photodegradation of RB is shown in Fig. 6c. It can be observed that the band around 538 nm drops gradually and tends to completely vanish after 120 min of irradiation which is due to the aromatic ring opening of RB which provides a pathway for degradation [38].

The degradation of MO (Fig. 6b) for ZnO nanoparticles are around 35%, 65%, 75%, and 96% at 30, 60, 90, and 120 min, respectively. Whereas the degradation of RB (Fig. 6d) are around 50%, 70%, 85.7%, and 90% at 30, 60, 90, and 120 min, respectively. The enhancement of photocatalytic degradation may be attributed to the increase in surface area due to the decreasing particle size [39, 40, 41]. Table 1 gives a comparison of the photocatalytic responses for various catalysts using different dyes.

4.6 Corrosion studies

The electrochemical impedance spectra or Nyquist plot for uncoated and ZnO nanoparticles coated Zn metal surfaces is shown in Fig. 7a. At low frequencies, a semicircle was obtained within the Nyquist plot diagram, which might be linearly involving the charge transfer resistance of the reaction (associated
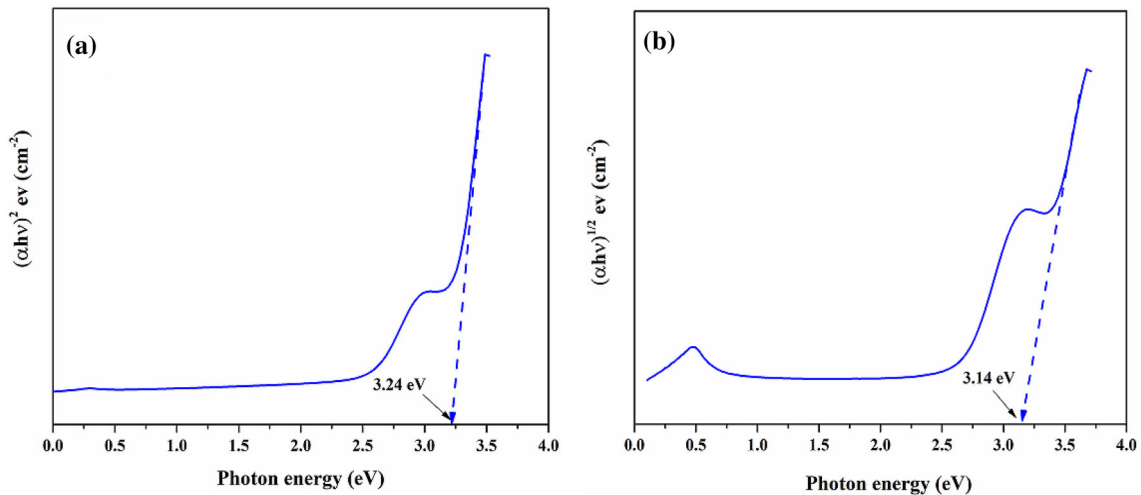
Fig. 3 **a**, **b** Tauc plot of the synthesized ZnO Nanoparticles
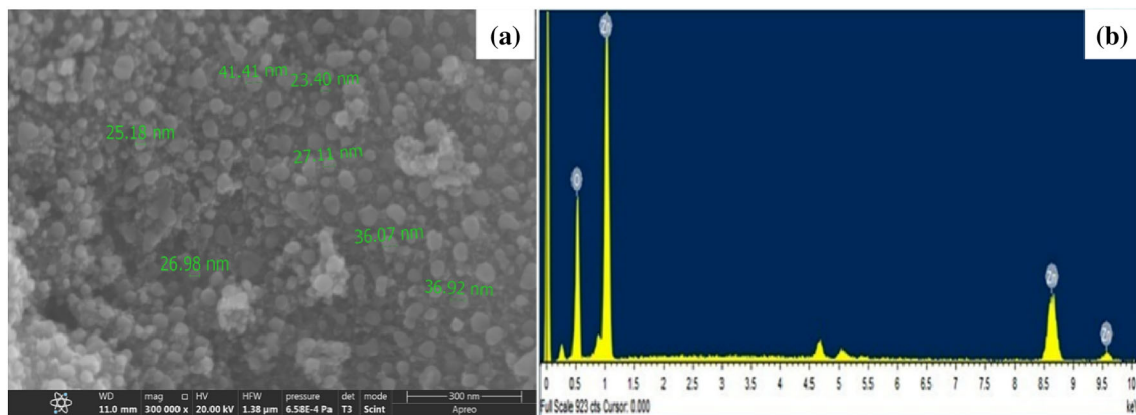

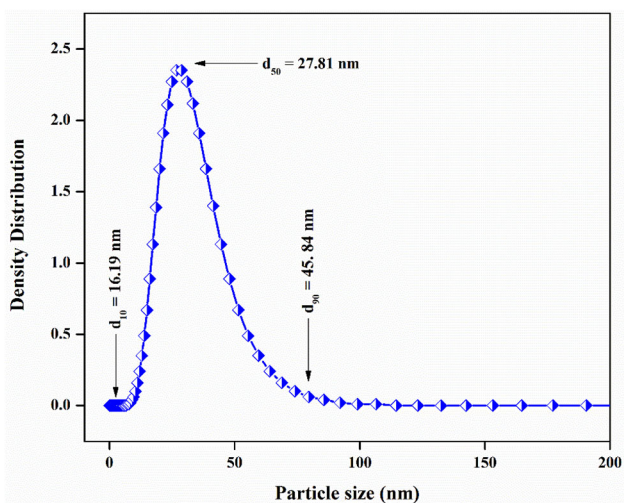**Fig. 4** **a** SEM micrographs, **b** EDX studies for the prepared ZnO nanoparticles

Fig. 5 Particle size distribution of the prepared ZnO nanoparticles

with the corrosion process). In Fig. 7a each sample show semi-circles (an electrical phenomenon loop), however, their radius varies noticeably. The ZnO nanoparticles coated Zn metal plate had higher electrical phenomenon values than the blank Zn metal samples, indicating that the coated samples have higher barrier properties against corrosion. The high Rct values for ZnO nanoparticles coated Zn plates signify the higher corrosion resistance of the metal surface.

Tafel plots or Potentiodynamic Polarization studies are carried out to analyze the electrochemical corrosive characteristics of a metal surface [42–44]. The Tafel plot for Zn metal plates and ZnO nanoparticles coated Zn metal plates in 3.5% NaCl solution is shown in Fig. 7b.

The potential was applied from − 1.4 V to 0 V and the corrosion of the Zn plate begins from the anode
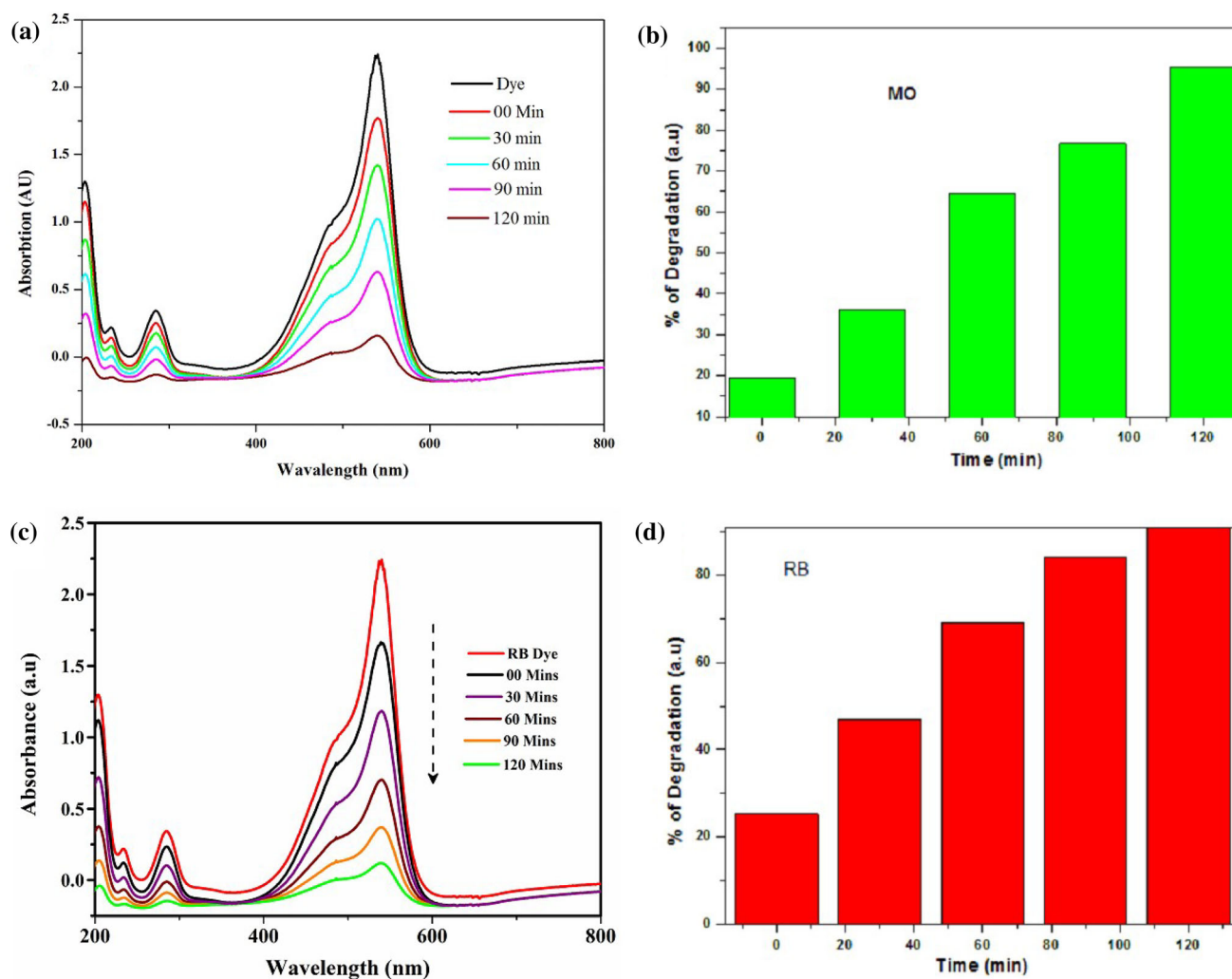
Fig. 6 **a**, **b** Photocatalytic degradation studies for ZnO nanoparticles by using methyl orange dye solution, **c**, **d** Rhodamine-B dye solution

Table 1 Comparison on the photocatalytic responses for different dyes

| Name of the source	Photocatalyst	Dye	Dye concentration (mgL^{-1})	Reaction time (mins)	Degradation efficiency (%)	References
Neem	ZnO	Rhodamine B	10	120	96.1	This work
		Methyl orange	10	120	85.7	
Delonix elata	SnO_2/MW	Rhodamine B	20	150	92.47	[31]
Moringa Oleifera	CuO	Pararosaniline	10	40	96.4	[35]
Sugar cane	SnO_2	Methylene blue	10	360	56.8	[39]
Sechium edule	ZnO	RB 160	50	120	96	[40]
Panax ginseng	ZnO	Methylene blue	15	80	99	[41]
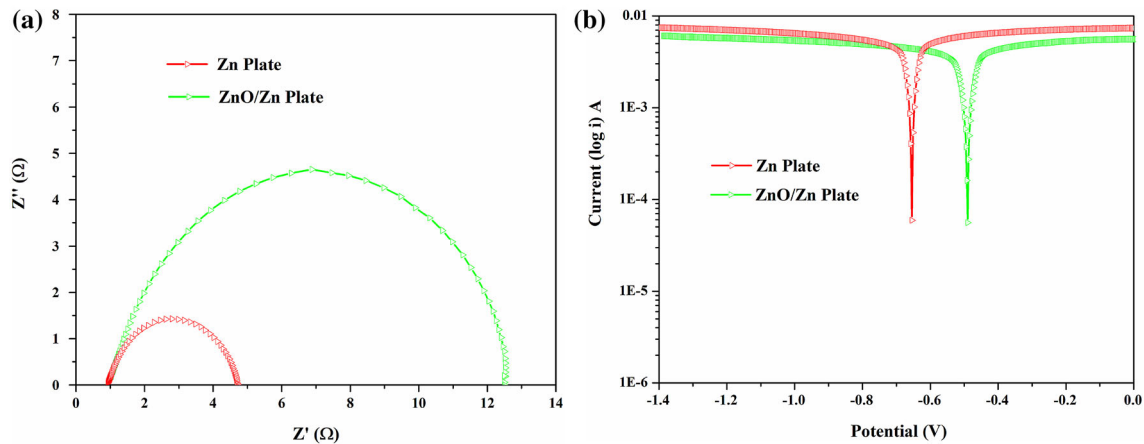
Fig. 7 **a** Nyquist plot and **b** Tafel plot of uncoated and ZnO nanoparticles coated Zn metal plates in 3.5% NaCl electrolyte

side which is consistent with the Tafel plot. From the Tafel plot, the potential of the ZnO nanoparticles coated plate is shifting toward the positive region (toward the anode side) in comparison with the uncoated Zn metal plate.

The Tafel plot shows that the ZnO/Zn plate contains a lower current density than the uncoated Zn plate. The comparison of corrosion current and corrosion potential for uncoated and ZnO coated Zn plates are illustrated from the results of the Tafel plot in Table 2. The corrosion efficiency rate for the ZnO/Zn plate seems to be around 50.11% higher in comparison with the uncoated Zn metal plate. The comparative assessment on the coating of nanomaterial

for various metal surfaces to improve its corrosion inhibition behavior is shown in Table 3.

5 Conclusion

Neem plant extracts were used to prepare Zinc oxide nanoparticles by adopting green synthesis methods. X-ray diffraction studies confirmed the single-phase formation of the compound without any impurities. SEM micrographs revealed that the prepared nanoparticles were spherically shaped with sizes ranging from 23 to 40 nm and the average size was confirmed from DLS studies. The bandgap of the prepared nanoparticles from UV–Vis analysis is

Table 2 Corrosion potential (E_{corr}) and corrosion current (I_{corr}) determined from Tafel plots of ZnO nanoparticles in 3.5% NaCl electrolyte

Substrate	Ecorr (mV)	Icorr (µA/cm^2)	Polarization resistance (Ω)	Corrosion rate (mm/year)	Improved efficiency
Zn plate	− 0.660	984.09	5.5118	11.435	–
ZnO/Zn plate	− 0.494	822.03	12.372	05.704	50.11%

Table 3 The comparative assessment on the coating of nanomaterial on different metal surfaces for improvement of corrosion inhibition behavior

S.No.	Inhibitor	Subtract	Medium	Corrosion inhibition efficiency (%)	Reference
1	ZnO	Zn	3.5% NaCl	50.1	This work
2	CuO	Mild steel	3.5% NaCl	53.57	[35]
3	NiO	Zn	3.5% NaCl	68.4	[42]
4			1 M HCl	75.7	
5	NiO	Mg	3.5% NaCl	61.10	[42]
6			6 M KOH	55.90	
7	MnO$_2$	Mild steel	1 M HCl	51.50	[43]
8	ZrO2	316L SS	1 M H$_2$SO$_4$	69.1	[44]

found to be around 3.1–3.3 eV. Photodegradation studies proved the better photocatalytic behavior for Rhodamine-B solution. The corrosion efficiency rate for the ZnO nanoparticles coated Zn plates were greater in comparison with the uncoated Zn plates.

Author contributions

SR: writing original draft, conceptualization and analysis. SS: data collection and analysis, writing review draft. DSK: conception and design of review draft. GM: analysis and writing review draft. MK and SK: material synthesis and data collection. SM and SM: data collection and analysis.

Data availability

Data would be provided by corresponding author upon the acceptance of the paper.

Declarations

Conflict of interest The authors declare that they have no conflict of interest.

Consent for publication The paper has been written by the above stated authors who are all aware of its content and approve its submission has not been published previously. It is not under consideration for publication elsewhere, no conflict of interest exists and if accepted the article will not be published elsewhere in the same form, in any language without the written consent of the publisher.

References

1. H. Liu, H. Liu, J. Yang, H. Zhai, X. Liu, H. Jia, Microwave-assisted one-pot synthesis of Ag decorated flower-like ZnO composites photocatalysts for dye degradation and NO removal. Ceram. Int. **45**(16), 20133–20140 (2019)
2. S. Fujihara, H. Naito, T. Kimura, Visible photoluminescence of ZnO nanoparticles dispersed in highly transparent MgF2 thin-films via sol-gel process. Thin Solid Films **389**, 227–232 (2001)
3. M. Stan, A. Popa, D. Toloman, A. Dehelean, I. Lung, G. Katona, Enhanced photocatalytic degradation properties of zinc oxide nanoparticles synthesized by using plant extracts. Mater. Sci. Semicond. Process. **39**, 23–29 (2015)
4. M. Murali, C. Mahendra, N. Rajashekar, M.S. Sudarshana, K.A. Raveesha, K. N. Amruthesh, Antibacterial and antioxidant properties of biosynthesized zinc oxide nanoparticles from *Ceropegia candelabrum* L.—an endemic species. Spectrochim. Acta Part A Mol. Biomol. Spectrosc. **179**, 104–109 (2017)
5. H. Agarwal, S.V. Kumar, S. Rajeshkumar, A review on green synthesis of zinc oxide nanoparticles—an eco-friendly approach. Resour. Technol. **3**, 406–413 (2017)
6. T. Bhuyan, K. Mishra, M. Khanuja, R. Prasad, A. Varma, Biosynthesis of zinc oxide nanoparticles from *Azadirachta indica* for antibacterial and photocatalytic applications. Mater. Sci. Semicond. Process. **32**, 55–61 (2015)
7. M. Ramesh, M. Anbuvannan, G. Viruthagiri, Green synthesis of ZnO nanoparticles using *Solanum nigrum* leaf extract and their antibacterial activity. Spectrochim. Acta Part A Mol. Biomol. Spectrosc. **136**, 864–870 (2015)
8. S. Ahmed, Saifullah, M. Ahmad, B. Swami, S. Ikram, Green synthesis of silver nanoparticles using *Azadirachta indica* aqueous leaf extract. J. Radiat. Res. Appl. Sci. **9**, 1–7 (2016)
9. M.H. Kahsay, A. Tadesse, D. RamaDevi, N. Belachew, K. Basavaiah, Green synthesis of zinc oxide nanostructures and investigation of their photocatalytic and bactericidal applications. RSC Adv. **9**(63), 36967–36981 (2019)
10. A. Sirelkhatim, S. Mahmud, A. Seeni, N.H.M. Kaus, L.C. Ann, S.K.M. Bakhori, H. Hasan, D. Mohamad, Review on zinc oxide nanoparticles: antibacterial activity and toxicity mechanism. Nano-Micro Lett. **7**, 219–242 (2015)
11. K. Vimala, S. Sundarraj, M. Paulpandi, S. Vengatesan, S. Kannan, Green synthesis of zinc oxide nanoparticles: a comparison. Process Biochem. **49**, 160–172 (2014)
12. P. Venkatachalam, M. Jayaraj, R. Manikandan, N. Geetha, E.R. Rene, N.C. Sharma, S.V. Sahi, Zinc oxide nanoparticles (ZnO NPs) alleviate heavy metal-induced toxicity in *Leucaena leucocephala* seedlings: a physiochemical analysis. Plant Physiol. Biochem. **110**, 59–69 (2017)
13. A.S.H. Hameed, C. Karthikeyan, A.P. Ahamed, N. Thajuddin, N.S. Alharbi, S.A. Alharbi, G. Ravi, In vitro antibacterial activity of ZnO and Nd-doped ZnO nanoparticles against ESBL producing *Escherichia coli* and *Klebsiella pneumonia*. Sci. Rep. **6**, 24312 (2016)
14. F. Movahedi, H. Masrouri, M.Z. Kassaee, Immobilized silver on surface-modified ZnO nanoparticles: as an efficient catalyst for synthesis of propargylamines in water. J. Mol. Catal. A: Chem. **395**, 52–57 (2014)
15. L. Martinkova, B. Uhnakova, M. Patek, J. Nesvera, V. Kren, Biodegradation potential of the genus *Rhodococcus*. Environ. Int. **35**, 162–177 (2009)
16. N. Jain, A. Bhargava, J. Panwar, Enhanced photocatalytic degradation of methylene blue using biologically synthesized

"protein-capped" ZnO nanoparticles. Chem. Eng. J. **243**, 549–555 (2014)

17. G. Bhumi, N. Savithramma, Biological synthesis of zinc oxide nanoparticles from *Catharanthus roseus* (L.) G. Don. Leaf extract and validation for antibacterial activity. Int. J. Drug Dev. Res. **6**, 208–214 (2014)

18. P.C. Nagajyothi, T.V.M. Sreekanth, C.O. Tettey, Y.I. Jun, S.H. Mook, Characterization, antibacterial, antioxidant, and cytotoxic activities of ZnO nanoparticles using Coptidis Rhizoma. Bioorg. Med. Chem. Lett. **24**, 4298–4303 (2014)

19. M. HassaniSangani, M. NakhaeiMoghaddam, M.M. Forghanifard, Inhibitory effect of zinc oxide nanoparticles on pseudomonas aeruginosa biofilm formation. Nanomed. J. **2**, 121–128 (2015)

20. M.J. Haque, M.M. Bellah, M.R. Hassan, S. Rahman, Synthesis of ZnO nanoparticles by two different methods & comparison of their structural, antibacterial, photocatalytic and optical properties. Nano Express **1**(1), 010007 (2020).

21. M.F. Sohail, M. Rehman, S.Z Hussain, Z.E. Huma, G. Shahnaz, O.S Qureshi, T.J. Webster, Green synthesis of zinc oxide nanoparticles by Neem extract as multi-facet therapeutic agents. J. Drug. Deliv. Sci. Technol. **59**, 101911 (2020)

22. V. Jeeva Lakshmi, R. Sharath, M.N. Chandraprabha, E. Neelufar, A. Hazra, M. Patra, Synthesis, characterization and evaluation of antimicrobial activity of zinc oxide nanoparticles. J. Biochem. Technol. **3**(5), S151–S154 (2012)

23. S.I. Durowaye, V.O. Durowaye, B.M. Begusa, Corrosion inhibition of mild steel in acidic medium by methyl red (2,4-dimethylamino-2′-carboxylazobenzene). Int. J. Eng. Res. Technol. **4**, 469–475 (2014)

24. J.J. Fu, H.S. Zang, Y. Wang, S.N. Li, T. Chen, X.D. Liu, Experimental and theoretical study on the inhibition performances of quinoxaline and its derivatives for the corrosion of mild steel in hydrochloric acid Ind. Eng. Chem. Res. **51**, 6377–6386 (2012)

25. M. Nasibi, M. Mohammady, E. Ghasemi, A. Ashrafi, D. Zaarei, G. Rashed, Corrosion inhibition of mild steel by nettle (*Urtica dioica* L.) extract: polarization, EIS, AFM, SEM and EDS studies. J. Adhes. Sci. Technol. **27**, 1873–1885 (2013)

26. S.A. Umoren, E.E. Ebenso, P.C. Okafor, O. Ogbobe, Water-soluble polymers as corrosion inhibitors. Pigment Resin. Technol. **35**, 346–352 (2006)

27. K.R. Basavalingiah, S. Harishkumar, G. Nagaraju, D. Rangappa, Highly porous, honeycomb like Ag–ZnO nanomaterials for enhanced photocatalytic and photoluminescence studies: green synthesis using Azadirachta indica gum. SN Appl. Sci **1**(8), 1–13 (2019)

28. P. Makuła, M. Pacia, W. Macyk, How to correctly determine the band gap energy of modified semiconductor photocatalysts based on UV–Vis spectra. J. Phys. Chem. Lett. **9**(23),

6814–6817 (2018). https://doi.org/10.1021/acs.jpclett.8b02892

29. V. Kavitha, J. Mayandi, P. Mahalingam, N. Sethupathi, Structural, optical and electrical studies on zinc doped barium strontium titanate as photo-anode for DSSC device. Mater. Today: Proc. **35**(1), 48–52 (2021)

30. V. Kavitha, P. Mahalingam, M. Jeyanthinath, N. Sethupathi, Optical and structural properties of tungsten-doped barium strontium titanate. Mater. Today: Proc. **23**(1), 12–15 (2020)

31. K.C. Suresh, S. Surendhiran, P. Manoj Kumar, E. Ranjth Kumar, Y.A. Syed Khadar, A. Balamurugan, Green synthesis of SnO2 nanoparticles using *Delonix Elata* leaf extract: evaluation of its structural, optical, morphological and photocatalytic properties. SN Appl. Sci. **2**, 1–13 (2020). https://doi.org/10.1007/s42452-020-03534-z

32. A. Berni, M. Mennig, H. Schmidt, Doctor blade, in *Sol–gel technologies for glass producers and users*. ed. by M.A. Aegerter, M. Mennig (Springer, Boston, 2004)

33. T. Roisnel, J. Rodriguez-Carvajal, WinPLOTR: a windows tool for powder diffraction patterns analysis. Mater. Sci. Forum **378**, 118–123 (2001)

34. Rodríguez-Carvajal, J. Recent advances in magnetic structure determination by neutron powder diffraction. Phys. B: Condens. Matter 192(1–2), 55–69 (1993)

35. S. Surendhiran, V. Gowthambabu, A. Balamurugan, M. Sudha, V.B. Senthil Kumar, K.C. Suresh, Rapid green synthesis of CuO nanoparticles and evaluation of its photocatalytic and electrochemical corrosion inhibition performance. Mater. Today: Proc. **47**(4), 1011–1016 (2021)

36. C.B. Ong, L.Y. Ng, A.W. Mohammad, A review of ZnO nanoparticles as solar photocatalysts: synthesis, mechanisms and applications. Renew. Sustain. Energy Rev. **81**, 536–551 (2018)

37. T. Bhuyan, K. Mishra, M. Khanuja, R. Prasad, A. Varma, Biosynthesis of zinc oxide nanoparticles from *Azadirachta indica* for antibacterial and photocatalytic applications. Mater. Sci. Semicond. Process. **32**, 55–61 (2015)

38. S.S.P. Selvin, N. Radhika, O. Borang, I.S. Lydia, J.P. Merlin, Visible light driven photodegradation of Rhodamine B using cysteine capped ZnO/GO nanocomposite as photocatalyst. J. Mater. Sci.: Mater. Electron. **28**(9), 6722–6730 (2017)

39. B. Archita, M. Ahmaruzzaman, Photocatalytic-degradation and reduction of organic compounds using SnO2 quantum dots (via green route) under direct sunlight. RSC Adv. **5**, 66122–66133 (2015). https://doi.org/10.1039/C5RA07578E

40. N. Elavarasan, K. Kokila, G. Inbasekar, V. Sujatha, Evaluation of photocatalytic activity, antibacterial and cytotoxic effects of green synthesized ZnO nanoparticles by *Sechium edule* leaf extract. Res. Chem. Intermed. **43**, 3361–3376 (2017). https://doi.org/10.1007/s11164-016-2830-2

41. L. Kaliraja, J.C. Ahna, E.J. Rupa, S. Abid, J. Lu, D.C. Yang, Synthesis of panos extract mediated ZnO nano-flowers as photocatalyst for industrial dye degradation by UV illumination. J. Photochem. Photobiol. B: Biol. **199**, 111588 (2019)

42. M. Sudha, S. Surendhiran, V. Gowthambabu, A. Balamurugan, R. Anandarasu, Y.A. Syed Khadar, D. Vasudevan, Enhancement of corrosive resistant behavior of Zn and Mg metal plates using biosynthesized nickel oxide nanoparticles. J. Bio Tribo-Corro. **7**, 60 (2021). https://doi.org/10.1007/s40735-021-00492-w

43. Y.A. Syed Khadar, S. Surendhiran, V. Gowthambabu, S. Halimabi Alias ShakilaBanu, V. Devabharathi, A. Balamurugan, Enhancement of corrosion inhibition of mild steel in acidic media by green-synthesized nano-manganese oxide. Mater. Today: Proc. **47**(4), 889–893 (2021)

44. N. Esmaiel, S. Mohammad, R. Hamid Reza, T. Fatemeh, Investigation of structural evolution and electrochemical behaviour of zirconia thin films on the 316L stainless steel substrate formed via sol–gel process. Surf. Coat. Technol. **205**, 5109–5115 (2011). https://doi.org/10.1016/j.surfcoat.2011.05.024